RELEASE OF DYNAMICALLY SCALED OBJECTS FROM A HELICOPTER WIND TUNNEL MODEL

K.H. Lammers*, I. Philipsen**, M.H. Ryu***
*NLR, **DNW, ***KAI

Keywords: *Dynamical, Store, Separation, Froude, SPR*

Abstract

KAI contracted NLR to explore safe conditions under which objects can be dropped from a helicopter wind tunnel model in the DNW-LST. Objects are manufactured with rapid prototyping that comply with both geometrical and dynamical scaling laws. Trajectories are measured optically and repeated drops resulted in reproduced trajectories. For some trajectories unsteady aerodynamic forces are determined.

1 General Introduction

In emergency situations it can occur that modern helicopters have to drop objects like fuel tanks to quickly reduce weight. When objects are dropped from a helicopter, there is a risk of the objects impacting the helicopter. This risk increases at larger angles of attack and sideslip. Therefore safe conditions under which objects can be dropped need to be explored in order for a helicopter to be operated safely in some extreme conditions.

The Korea Aerospace Industries Co. LTD (KAI) develops a wide range of helicopters. KAI contracted the Netherlands Aerospace Centre (NLR) to measure trajectories from objects dropped from a 1:8.5 scaled helicopter wind tunnel (WT) model used in earlier wind tunnel tests. The wind tunnel test was performed at the Low-Speed Tunnel (LST) of the German-Dutch Wind Tunnels (DNW) using an optical tracking system to accurately capture the objects trajectory.

1.1 Scaling Laws

The trajectories of the 1:8.5 geometrically scaled objects should represent the trajectories of the full scale objects. This means that all forces acting on the model scale object should be scaled proportional [1]. In this experiment these forces are gravity and aerodynamic forces, hence:

$$\frac{Fg_s}{Fg_m} = \frac{Fa_{fs}}{Fa_m} \qquad (1)$$

In the equation above *Fg* stands for the gravitational force and *Fa* for aerodynamic force. The subscript *fs* and *m* denote the full scale and model scale respectively.

Three different scaling methods were considered before manufacture of the objects: Froude Scaling (FRS), Light Body Scaling (LBS) and Heavy Body Scaling (HBS). For this test only low full scale Mach numbers (M) up to 0.25 were planned. When, as in this case, compressibility effects are minor, FRS is typically used because of the smaller scaling factors involved with this method in comparison with LBS and HBS [2].

FRS implies that the full scale and model scale Froude number (Fr) are the same. This similarity parameter is defined as the ratio of flow inertia to external force field and is given in equation 2.

$$Fr = \frac{V}{\sqrt{g \cdot L}} \qquad (2)$$

where *V* is the velocity of the flow, *g* stands for an external force field (i.e. in this case gravity) and *L* is a characteristic length.

The scaled airspeed for the wind tunnel test can now be derived following FRS:

$$\begin{aligned} Fr_{fs} &= Fr_m \\ \frac{V_{fs}^2}{g \cdot L_{fs}} &= \frac{V_m^2}{g \cdot L_m} \\ \frac{V_{fs}^2}{g \cdot \lambda \cdot L_m} &= \frac{V_m^2}{g \cdot L_m} \\ V_m &= \lambda^{-1/2} \cdot V_{fs} \end{aligned} \quad (3)$$

The scale factor, λ, is in this case 8.5. With help of equation 3, time scaling can be derived:

$$\begin{aligned} V_m &= \lambda^{-1/2} \cdot V_{fs} \\ \frac{L_m}{t_m} &= \lambda^{-1/2} \cdot \frac{\lambda \cdot L_m}{t_{fs}} \\ t_m &= \lambda^{-1/2} \cdot t_{fs} \end{aligned} \quad (4)$$

In a similar way other relevant parameters can be derived. The FRS scaling of relevant parameters is given in Table 1.

Table 1. Relevant scaled parameters.

Geometry	$L_m = \lambda^{-1} \cdot L_{fs}$
Mass	$m_m = \rho_m \cdot \rho_{fs}^{-1} \cdot \lambda^{-3} \cdot m_{fs}$
Mass inertia	$I_{ij,m} = \rho_m \cdot \rho_{fs}^{-1} \cdot \lambda^{-5} \cdot I_{ij,fs}$
Ejector force	$Fe_m = \rho_m \cdot \rho_{fs}^{-1} \cdot \lambda^{-3} \cdot Fe_{fs}$
Aerodynamic force	$Fa_m = \rho_{air,fs} \cdot \rho_{air,m}^{-1} \cdot \lambda^{-3} \cdot Fa_{fs}$
Flow velocity	$V_m = \lambda^{-1/2} \cdot V_{fs}$
Body velocity	$U_m = \lambda^{-1/2} \cdot U_{fs}$
Acceleration	$a_m = a_{fs}$
Angular velocity	$\dot{\theta}_m = \lambda^{1/2} \cdot \dot{\theta}_{fs}$
Angular acceleration	$\ddot{\theta}_m = \lambda \cdot \ddot{\theta}_{fs}$
Time	$t_m = \lambda^{-1/2} \cdot t_{fs}$

It is possible to take altitude scaling into account through proper scaling of object density. To do so, equation 1 can be rewritten to obtain proper scaling relations.

$$\begin{aligned} \frac{\rho_{fs} \cdot B_{fs} \cdot g}{\rho_m \cdot B_m \cdot g} &= \frac{1/2 \cdot \rho_{air,fs} \cdot V_{fs}^2 \cdot S_{fs} \cdot c}{1/2 \cdot \rho_{air,m} \cdot V_m^2 \cdot S_m \cdot c} \\ \frac{\rho_{fs} \cdot \lambda^3 \cdot B_m \cdot g}{\rho_m \cdot B_m \cdot g} &= \frac{1/2 \cdot \rho_{air,fs} \cdot \lambda \cdot V_m^2 \cdot \lambda^2 \cdot S_m \cdot c}{1/2 \cdot \rho_{air,m} \cdot V_m^2 \cdot S_m \cdot c} \\ \frac{\rho_{fs}}{\rho_m} \cdot \lambda^3 &= \frac{\rho_{air,fs}}{\rho_{air,m}} \cdot \lambda^3 \end{aligned} \quad (5)$$

where ρ is the object density and ρ_{air} is the air density, B is the object volume, S is the object surface and c is the aerodynamic force coefficient. This test is designed to simulate emergency situations where rapid weight reduction through object release is necessary. These situations in general occur at very low altitude i.e. sea level. Therefore $\rho_{air,fs}=\rho_{air,m}$, this implies that the density of the model scale and full scale object should also be the same. As a result all density ratios in Table 1 are equal to unity.

The full scale helicopter has a passive ejector, therefore $Fe=0$. For the remainder of this paper dimensions are given in model scale, except if explicitly mentioned otherwise.

2 Test set-up

A 1:8.5 scaled helicopter wind tunnel model was used during this test. The rotor of this wind tunnel model was removed so that the model could be suspended from the ceiling of the test section. Wake coming from the rotor is therefore not included in the wind tunnel test.

For a few test points the angle of attack was not equal to zero. The trajectories measured during these test points are not representative for real flight since the direction of the gravitation vector is incorrect with respect to the flow vector.

The objects are highly detailed and are therefore manufactured with state-of-the-art rapid prototyping.

An non-intrusive optical measurement system is used to measure the trajectories. This optical measurement systems is capable of measuring all 6 degrees of freedom (DOF) of the dropped objects by using stereo pattern recognition (SPR). The floor of the test section was covered with acoustic foam to prevent the store from damage during the test. A flexible net was placed downstream to prevent the objects from being blown too far downstream, see Figure 1. Before the test a dedicated calibration of the test section including foam and net was performed to take any effects of these risk mitigations into account.

2.1 Manufacturing

Two types of objects are manufactured, from here on referred to as object #1 and object #2. Both objects can have different configurations (empty, almost empty, almost full, full, symmetrically partially full, asymmetric, etc.). Only completely full or completely empty configurations will be discussed in this paper. Object #1 has a cylindrical shape and object #2 has a shape of two horizontally parallel cylinders. Boxes enclosing the objects can be drawn and are shown in Figure 1.

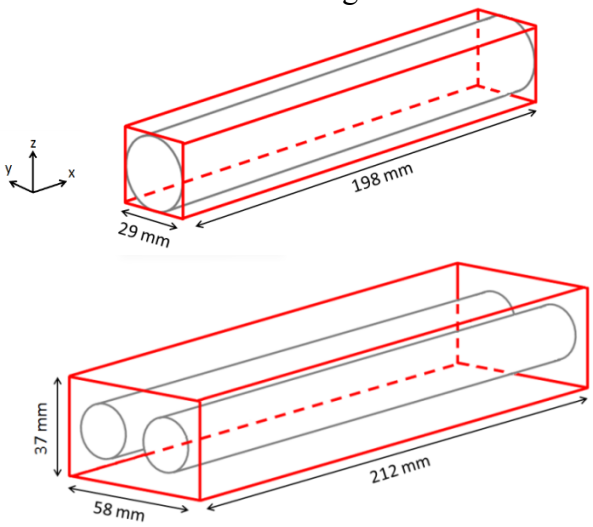

Figure 1. Schematic view of object #1 (top) and object #2 (bottom) with enclosing boxes.

The figure above only shows a schematic view of the objects because of confidentiality reasons, the real objects contain much more detail.

The objects are designed using computer 3D-modelling. In the design process much effort is spend on obtaining the correct mass, mass inertia and center of gravity (CoG). After completing the design, the objects were manufactured. Mass, longitudinal CoG and mass inertia were measured to inspect the accuracy of the manufacturing process. FRS scaled masses of the objects were in the range of 25 to 100 grams. Deviations between FRS scaled masses and masses of the manufactured objects were around 1%. The CoG of the manufactured objects was in the same accuracy range. The FRS scaled mass inertia of the objects could be manufactured within 5% accuracy.

2.1.2 Measuring mass, CoG and mass inertia

Mass and CoG are determined by using two laboratory scales, see Figure 2.

Figure 2. Measuring mass and CoG.

Mass of the manufactured object is within 1% accuracy with respect to its FRS value, with a maximum measuring uncertainty of 0.04% of the FRS value. CoG of the manufactured object is within 1.5% accuracy with respect to its FRS value, with a maximum measuring uncertainty of 0.9% of the FRS value.

A bifilar torsional pendulum method [3] was used to measure mass inertia of the objects. In this method the model is hung between two parallel filaments and the rotational mass inertia is determined from the equation of motion for a pendulum. The oscillating motion was captured with 200 frames per second (fps), using a high speed camera. The results of the conventional linear approximations were compared to the results using the non-linear equation of motion of the oscillator. The non-linear method takes account of the damping effects of the pendulum moving in air [4]. The longitudinal mass inertia of the manufactured object is within 4% accuracy with respect to its FRS value, the maximum uncertainty in the pendulum method is for the longitudinal axis is 1% [5].

The mass inertia around some axes were not measured because of symmetry or because of the relatively short horizontal distance between the two parallel filaments in the pendulum method, causing high measurement errors.

2.1.3 Release mechanism

The full scale helicopter separates the objects by opening two clamps. The wind tunnel model is too small to incorporate fully working clamps,

instead the clamps are modelled as static parts and for the release mechanism a release hook is designed. The release hook and release clamps are shown in Figure 3.

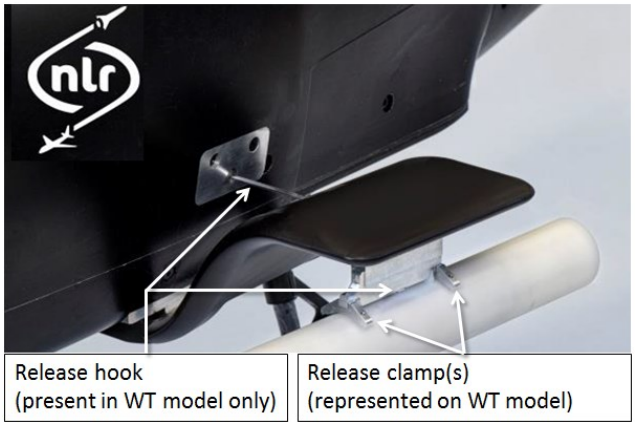

Figure 3. Full scale and model scale release mechanism.

The working principle of the release hook is depicted in Figure 4. With this release hook the initial condition of *Fe=0* is realized. The full scale separator is incorporated as a passive part in the wind tunnel model, which is important because the object may touch the clamps right after release, thereby influencing the trajectory. Under the condition that the objects don't touch the release hook after separation, the separation process is properly simulated.

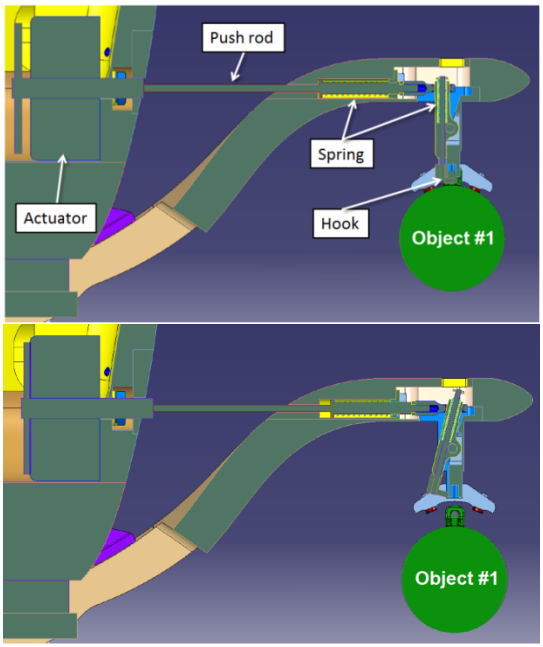

Figure 4. Release mechanism just for release (top) and just after release (bottom).

2.2 Measurement Technique

The object trajectories are captured with the Stereo Pattern Recognition measurement technique [6]. The SPR measurement equipment consists of two or three Mikrotron EoSens CoaXPRess 4CXP 4 Megapixel cameras (2336x1728 pixel @ 560 fps) with 12 mm Kowa objective lenses and an adapted computer with software and equipment. Since the DNW-LST has easy optical access, the cameras are located outside the wind tunnel. On the objects a unique pattern of fluorescent markers is applied. This marker pattern is unique in the sense that the distance between any marker pair is unique. During a measurement, the wind tunnel is illuminated by UV light only. Filters before the camera lenses ensure that only light of the wavelength reflected by the markers is entering the cameras. About one second of data is recorded. The recording is triggered by the activation of the release mechanism. The number of frames before full retraction of the release hook was established prior to the test. This implies that also the initial location and attitude of the object is recorded during a measurement. The camera set-up is calibrated using a so-called calibration frame with markers on it, of which the location is precisely known. The camera set-up is calibrated with respect to the wind tunnel coordinate system. The uncertainty in the individual obtained marker location is estimated at 0.025 mm in x- and z-direction, and it is 0.06 mm in y-direction. The larger uncertainty for the y-directions is due to the chosen two camera arrangement. A right hand coordinate system is used. The x-direction is in stream wise direction, the z-direction in vertical direction (upward positive) and y-direction is in lateral direction.

The generation of final SPR data, thus the determination of x-, y- and z-location of every visible marker on the surface of the store is performed in the post processing phase after each data point is taken. Therefore, the CCD camera images are searched for marker images. Correspondence between the CCD-image and marker images is established using epipolar line searches. The cameras form a set of stereoscopic pairs. After image correspondences have been

established a point clouds is reconstructed. Since the pattern of the markers is unique (and known) the location and attitude of the store can be calculated. To do so, at least three uniquely identifiable markers have to be located. Since it is not known which markers are visible to the camera, a search algorithm is applied. By using just two cameras it is apparent that when the x-axis of the object is closely aligned with view axis of one of the cameras, the location of the markers cannot be established precise enough. The object is in such a case “invisible” for the SPR system. This can be circumvented by the use of three or four cameras.

Once it is clear which markers on the store are visible, the transformation matrix can be established that corresponds to this situation. Out of this transformation matrix the location of the store can be determined and the rotational matrix can be determined. Since the attitude of an object can be attained in more than one way, the order of rotation around the stores axis is of importance. For completeness, the rotational matrix is also made available in the data.

3 Results and analysis

The main objective of this wind tunnel test is to explore the range of safe conditions to perform emergency store separation. In addition an attempt was made to determine unsteady aerodynamic forces and moments.

Video recordings were processed into trajectory data. This data still contained some outliers. Outliers were removed and replaced with fitted data points by using a moving average filter (with a stencil size of 5 frames). A data point was identified as outlier when the residue between data point and fitted value was more than 6 times the median value of all residues for that trajectory.

For some frames it was not possible to determine the position and attitude of the object, resulting in ‘missing frames’ in the trajectory. The missing frames were filled up with linear interpolation.

3.1 Trajectories

In Figure 5 a repeat test point is shown for a case where the object hits the helicopter model (one run is depicted with a red line and asterisk markers, the other is depicted with blue and circle markers). The strike occurs around 0.12 seconds. This strike is a very unstable process, causing poor reproducibility in the subsequent part of the trajectory.

A similar repeat run for a case where the object does not hit the helicopter model is shown in Figure 6. For confidentiality reasons no values on the vertical axis are shown, but the vertical axis ranges for Figure 5 and Figure 6 are the same, for the position plots roughly 1000 mm and for the attitude plots roughly 400 degree. Very good reproducibility is achieved as can also be seen in Figure 7. Again, no values on the vertical axis can be shown, the range for the position plot vertical axis is roughly 60 mm and for the attitude plot roughly 15 degree. Similar reproducibility results are obtained with other repeat runs. This demonstrates proper functioning of the release mechanism, proper function of the measurement technique and quite stable flow around the helicopter. Both Figure 5 and Figure 6 show only the first 0.3 seconds of the drop to maintain axis limits that still make it possible to distinguish differences between runs. The trajectories are given in a helicopter aligned axis system and the airspeed is 16 m/s. These are trajectories from the empty object #1 configuration, which is relatively light, and therefore aerodynamic forces are dominant.

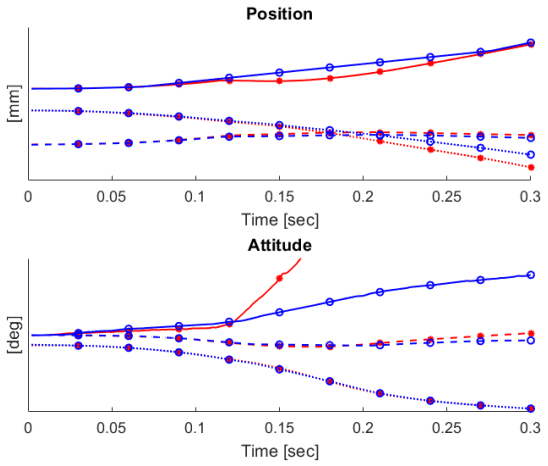

Figure 5. Two runs, object hits the WT model. Solid line is x-position/roll, dashed line is y-position/pitch, dotted line is z-position/yaw.

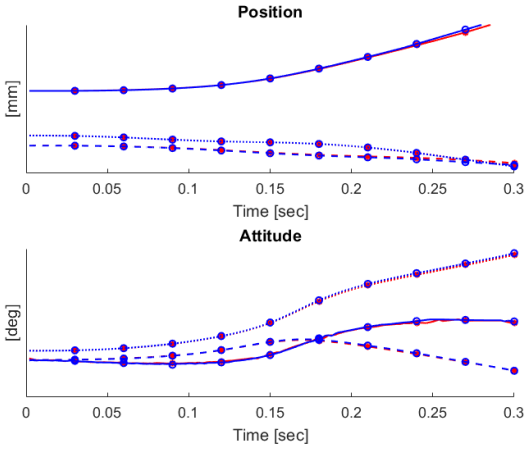

Figure 6. Two runs, object does not hit the WT model. Solid line is x-position/roll, dashed line is y-position/pitch, dotted line is z-position/yaw.

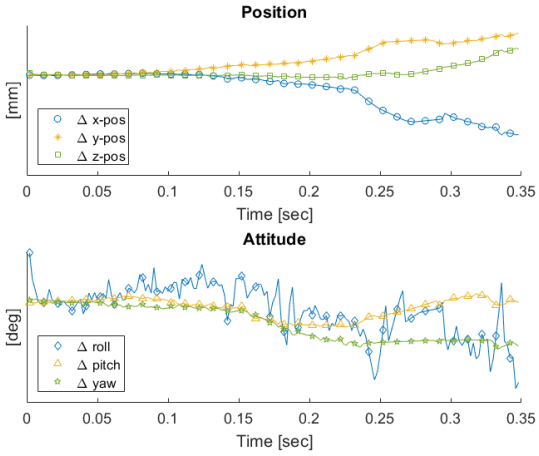

Figure 7. Difference between the two repeat runs of Figure 6.

The Cartesian coordinates of the trajectories are the coordinates of the object reference point (which is not the CoG because of different object configurations). With this object reference point and the store orientation it is possible to construct the boxes of Figure 1at every frame.

As an example to illustrate a typical set of 3D-trajectories, an angle of attack (AoA) sweep is constructed from several test points and shown in Figure 8. These are trajectories of the fully loaded object #1 configuration, which is relatively heavy and therefore dominated by gravity. The range of the vertical axis is roughly 1500 mm. The airspeed was 23 m/s and the trajectories are given in the helicopter aligned axis system.

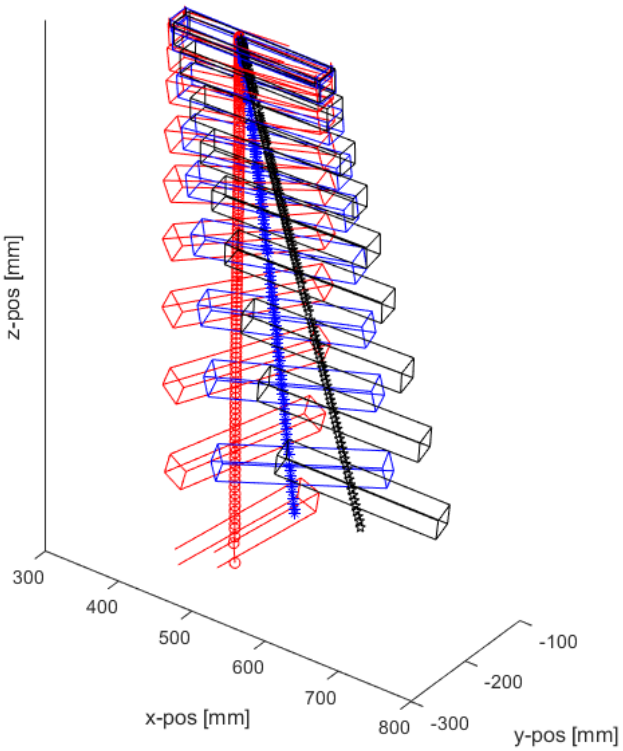

Figure 8. AoA-sweep of full object #1 box trajectory

A strike of the object onto the helicopter model can be identified during post processing. Strikes could also be identified during the test by replaying video recordings of the markers. A marker was also placed on the landing gear to visualize it in the recordings; this part was known to be a target for object impact. This strike identification approach increased the

effectiveness of the test in terms of exploring the safe range of separation conditions, see Figure 9.

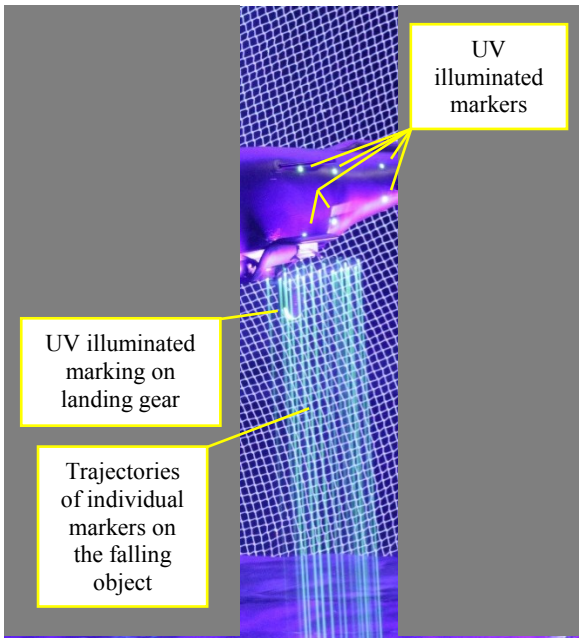

Figure 9: Photographic recording with long exposure time, markers on the model are clearly visible.

3.2 Unsteady aerodynamics

Unsteady aerodynamic forces and moments can be derived from trajectory data via the equations of motion of the objects. For derivation of the forces Newton's second law of motion in the form of equation 6 will be used.

$$\vec{F} = \frac{d}{dt}\left(m\vec{U}\right) + \vec{\omega} \times m\vec{U} \qquad (6)$$

where $\vec{F}=(F_x,F_y,F_z)^T$ is the external force vector, $\vec{U}=(u,v,w)^T$ is the object velocity vector and $\vec{\omega}=(p,q,r)^T$ is the angular velocity vector. All vectors of the equation above are defined in the object aligned axis system.

The external forces are the sum of aerodynamic forces and gravitational forces. The gravitation force, $\vec{W}$, is given in equation 7

$$\vec{W} = \begin{pmatrix} -mg\sin(\theta) \\ mg\sin(\phi)\cos(\theta) \\ mg\cos(\phi)\cos(\theta) \end{pmatrix} \qquad (7)$$

where θ is the roll angle, ϕ the pitch angle and ψ the yaw angle. Together they form the attitude vector, $\vec{\Phi}=(\theta,\phi,\psi)^T$. The aerodynamic force vector in object aligned axis system, $\vec{A}$, is then given as:

$$\vec{A} = \begin{pmatrix} m(\dot{u} + qw - rv) + mg\sin(\theta) \\ m(\dot{v} + ru - pw) - mg\sin(\phi)\cos(\theta) \\ m(\dot{w} + pv - qu) - mg\cos(\phi)\cos(\theta) \end{pmatrix} \qquad (8)$$

In a similar way the aerodynamic moments can be derived. The sum of external moments acting on a body must be equal to the time rate of change of its angular momentum:

$$\vec{M} = \frac{d\vec{H}}{dt} + \vec{\omega} \times \vec{H} \qquad (9)$$

$\vec{H}$ is the angular momentum vector in object aligned axis system, which is defined as:

$$\vec{H} = I\vec{\omega} \qquad (10)$$

where I is the 3x3 matrix containing the mass inertia of the object. The equations for the aerodynamic moments in object aligned axis system then become:

$$\begin{aligned} M_x &= \dot{p}I_x - \dot{q}I_{xy} - \dot{r}I_{xz} + qr\left(I_z - I_y\right) \\ &\quad - pqI_{xz} + prI_{xy} + (r^2 - q^2)I_{yz} \\ M_y &= -\dot{p}I_{yx} + \dot{q}I_y - \dot{r}I_{yz} + pr(I_x - I_z) \\ &\quad - qrI_{xy} + pqI_{yz} + (p^2 - r^2)I_{xz} \\ M_z &= -\dot{p}I_{zx} - \dot{q}I_{zy} + \dot{r}I_z + pq\left(I_y - I_x\right) \\ &\quad - prI_{yz} + qrI_{xz} + (q^2 - p^2)I_{xy} \end{aligned} \qquad (11)$$

The object velocity, acceleration, angular velocity and angular acceleration are needed to solve equation 8 and 11. These are calculated from the measured object positions and attitudes by using a 4th order accurate central finite difference scheme. The velocities and accelerations of equation 8 and 11 are defined in the object aligned axis system. The trajectories are measured in a tunnel aligned axis system. Therefore, transformation matrices have to be taken into account when determining velocities and accelerations in the object aligned axis system.

The measured trajectories contain some scatter and linear filled up holes of missing frames. This will blow up during numerical

differentiation, therefore smoothing is applied before differentiation. As first attempt to remove scatter, a low pass filter was applied. Unfortunately it was not possible to distinguish between measurement scatter and unsteady aerodynamics in the frequency domain. Instead a time domain filter had to be applied. All 6 DOF are independently smoothed, attempts with many filters were made including a simple linear Kalman filter. Finally the Savitzky-Golay filter yielded the best results, after some trial and error the most suitable stencil size and degree were determined. Smoothing is done in an iterative process till the maximum difference between two iteration steps is less than 0.1 mm or 0.1 degree. Smoothing is not continued further to prevent smoothing out the unsteady aerodynamics.

In Figure 10 the unsteady aerodynamic forces and moments of an empty object #2 trajectory with subsets of missing frames are presented (helicopter model AoA=8.5 deg, AoS=0 deg and V=24.7 m/s). The red data points correspond with missing frames. The missing frames are filled with linear interpolation, then smoothing is applied and finally the aerodynamic forces and moments are calculated. No values on the vertical axis are given because of confidentiality reasons, the vertical axis range of the loads plot is roughly 15 N and of the moments plot roughly 0.3 Nm. This linear interpolation causes very large accelerations to exist just before and after the interpolated part (even after smoothing), resulting in unreliable large aerodynamic forces and moments.

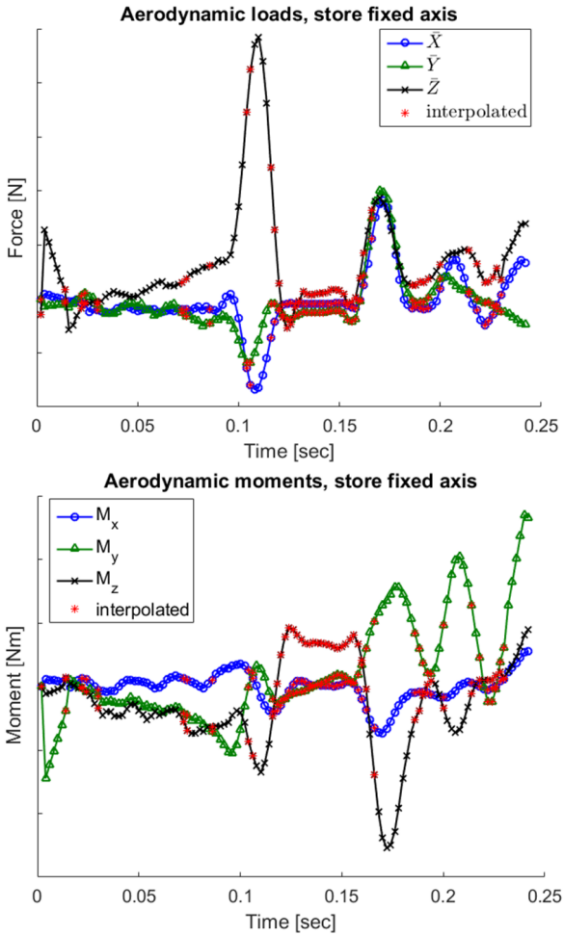

Figure 10. Unsteady aerodynamic forces and moments of a trajectory with subsets of missing frames (red asterisk)

A limited set of test points did not suffer from subsets of missing frames. An example of aerodynamic forces and moments derived from these test points is shown in Figure 11. No values are given on the vertical axis, but for the loads plot the vertical axis range is roughly 7 N and for the moments plot roughly 0.1 Nm. Both aerodynamic forces and moments still contain periodic behavior, possible related to the smoothing algorithm. General trends in Figure 11 can, however, be observed.

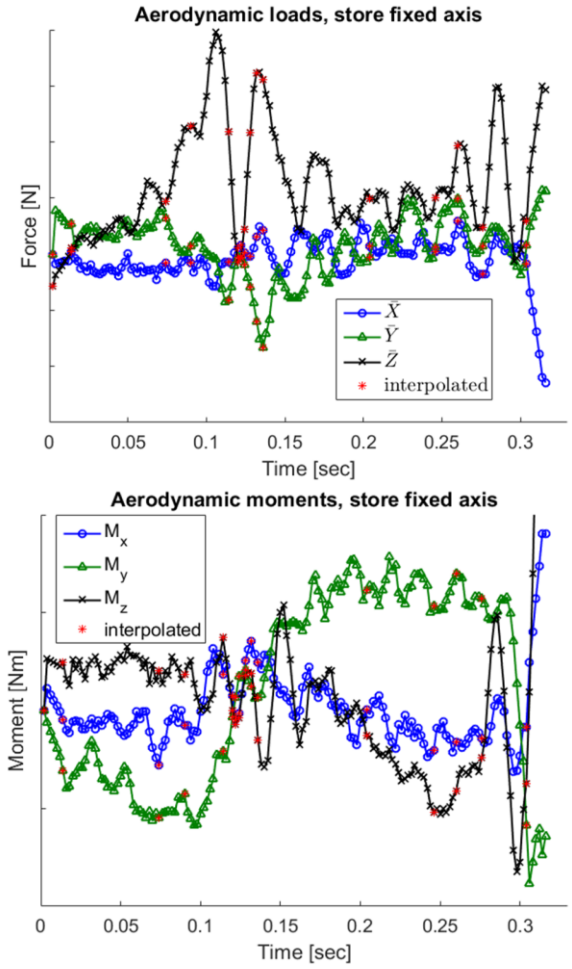

Figure 11. Unsteady aerodynamic forces and moments of a trajectory without large subsets of missing frames (red asterisk)

During the wind tunnel test free fall runs were performed (no wind). With these runs an uncertainty estimation of the test set-up can be derived. The general trend from free fall run is removed from the data, what remains is stochastic scatter. The uncertainties of the 6 DOF are given in Table 2. Note that the estimated uncertainty of the individual marker positions is different than that of the location and attitude of the store. The location and attitude of the store is obtained after post-processing all the marker positions, each with its own uncertainty. The uncertainty in roll angle is relatively large when compared to pitch and yaw. This can be explained by the fact that the orthogonal distance between the markers and the x-axis is shorter than the orthogonal distance between the markers and the y- or z-axis.

Table 2. Standard deviation of estimated uncertainty

x [mm]	y [mm]	z [mm]	ϕ [deg]	θ [deg]	ψ [deg]
0.06	0.16	0.13	0.10	0.04	0.06

4. Conclusions

KAI, NLR and DNW conducted a successful emergency store separation low speed wind tunnel test, using Froude dynamically scaled and 1:8.5 geometrically scaled objects dropped from a helicopter wind tunnel model.

Target mass, CoG and mass inertia were determined with Froude scaling. By making use of state-of-the-art 3D-modelling and rapid prototyping it was possible to manufacture objects that comply with the derived mass, CoG and mass inertia. A geometrically scale factor of 8.5 was used because of the already existing wind tunnel model. A smaller scale factor (larger wind tunnel model) can be used to increase manufacture accuracy.

The optical stereo pattern recognition system made it possible to accurately measure the trajectories of the store without causing any flow disturbance. With this measurement technique direct impact of the object on the helicopter was identified quickly, increasing the effectiveness of the test. A third camera can be used to reduce the number of missing frames. This camera is available for future wind tunnel tests. A larger wind tunnel model or smaller field of view will increase the accuracy of the measured marker positions. This is, however, not always desired since store separation tests often need relatively large fields of view.

An attempt was made to derive unsteady aerodynamic forces and moments from the trajectory data. General trends are successfully captured for a very limited set of trajectories. However, for most trajectories it was not possible to derive reliable aerodynamic forces and moments. The major cause for this is subsets of missing frames. By making use of more than two cameras the amount of missing frames can be reduced. The amount of scatter can be reduced by having a larger model scale or smaller field of view. To better distinguish

scatter from unsteady aerodynamics in the frequency domain, more frames per second can be used. However, this will also increase the required amount of UV-light to sufficiently illuminate the markers. Data post-processing can also be improved. For this test post-processing was performed partly by DNW and partly by NLR. DNW determined the trajectories and NLR tried to derive unsteady forces and moments from these trajectories. Better is to do the post-processing in one single step, involving more physics in the post-processing and handling the 6 DOF as a coupled system. Currently NLR and DNW are developing such post-processing software.

For this test trajectories were measured with satisfying accuracy, which was the main goal. For future testing an additional camera and improved post-processing software will be available, making reliable unsteady forces and moments measurements possible.

References

[1] Schindel L H. Store separation. *AGARD-OGRAPH-202*, No. 202, 1975

[2] Deslandes R M and Donauer S. Scaled-Drop-Tests: WYSIWYG or Not?. *48th AIAA Aerospace Sciences Meeting*, pp 2010-681, 2010.

[3] Shakoori A, Betin A V and Betin D A. Comparison of three methods to determine the inertial properties of free-flying dynamically similar models. *Journal of Engineering Science and Technology*, Vol. 11, No. 10, pp 1360-1372, 2016.

[4] Jardin M R and Mueller E R. Optimized measurements of unmanned-air-vehicle mass moment of inertia with a bifilar pendulum. *Journal of Aircraft*, Vol. 46, No. 3, pp 763-776, 2009.

[5] Meulen M P. Determination of rotational inertia using the bifilar pendulum method. *NLR-TR-2016-486*, Netherlands Aerospace Centre (NLR), Marknesse, 2016.

[6] Postma, J., Artois, K. and Philipsen, I. Wind Tunnel Test on the Breakthrough Laminar Aircraft Demonstrator Europe in the DNW-LLF, *53rd AIAA Aerospace Sciences Meeting*, pp 2015-1561, 2015.

8 Contact Author Email Address

mailto: karel.lammers@nlr.nl

Copyright Statement